Stochastic analysis of vortex-induced vibrations of two oscillating cylinders in the proximity-wake interference region

By G. Geraci, M.D. de Tullio† AND G. Iaccarino

1. Motivation and objectives

Vortex-induced vibrations (VIV) of structures is a phenomenon of great interest for a broad range of engineering fields. For instance, vortex shedding and vortex-excited oscillations may occur in marine structures such as risers and conductor tubes employed in oil drilling and production, deep water pipelines, or civil engineering structures such as bridges and chimney stacks. The paramount importance of this problem led to many research studies, both experimental and numerical (Borazjani & Sotiropoulos 2009; Griffin & Ramberg 1982). In literature, the flow past a single elastically mounted cylinder has received great attention since it has served as a prototype for VIV problems; however, this relatively simple system exhibits enough complexity to still be the subject of intense research (Williamson & Govarghan 2004). The picture is further complicated when a more realistic configuration is considered: two or more elastic structures are arranged in proximity to each other. Understanding the response of these kinds of structures is of a fundamental importance for safety and reliability when the mitigation of the VIV is a critical goal to achieve during the design. It is widely reported in the literature that a single elastically mounted cylinder, placed in a free stream, undergoes large amplitude oscillations when the shedding frequency synchronizes with the oscillation frequency (Williamson & Roshko 1988). Unlike the forced vibration behavior of a linear oscillator, here the vortex shedding synchronization occurs over a range of frequencies, called the lock-in region. The flow physics in this regime is much more complex than the von Karman vortex street, which appears for fixed bluff bodies. Further complexity arises when a second cylinder is placed in the wake of the front cylinder. Depending on the arrangement, namely tandem, staggered, or side by side, different critical distances can be identified to delimit regimes characterized by distinct mechanisms of interactions between cylinders. In particular, in this work we consider the case of a pair of cylinders placed in tandem (see Figure 1). We know from literature (Zdravkovich & Pridden 1977) that if the distance is large enough, namely $L/D > 4$, only the rear cylinder is affected by the presence of the front wake. On the contrary, if $L/D < 4$, then the front wake itself is sensible to the presence of the rear cylinder. This regime is called the proximity-wake interference region and is adopted as the nominal condition in the present work. More precisely, we refer to the configuration with $L_x/D = 1.5$. For this configuration, Borazjani & Sotiropoulos (2009) carried out an extensive numerical analysis for $Re = 200$, which they identified as the upper bound for which the flow remains essentially two-dimensional. Among other aspects, the authors identify larger amplitudes of motion and a lock-in region for the configuration in tandem with respect to the isolated cylinder and also the existence of a threshold in the reduced velocity which delimits the behavior of

† Politecnico di Bari, Bari, Italy

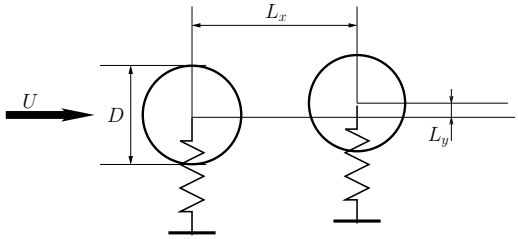

FIGURE 1. Schematic representation of the cylinders tandem arrangement and notation used.

the system. More precisely, for reduced velocities below the threshold, the amplitude of the front cylinder's oscillations exceeds that of the rear cylinder's oscillations, whereas above the threshold, the rear cylinder exhibits larger amplitudes of oscillation compared to the front one. The goal of the present work is to extend the study reported in Borazjani & Sotiropoulos (2009), including the quantification of the effect of an uncertain distance between the cylinders: a horizontal and a vertical separation are assumed to be uncertain parameters. We aim to quantify, in a probabilistic sense, the occurrence of the phenomena mentioned above, and reported in Borazjani & Sotiropoulos (2009), over a reduced velocity envelope. The remainder of the brief is organized as follows: in Section 2 the physical problem and the relevant governing equations are introduced. The numerical setting is described in Section 3, where we discuss both the deterministic solver (Section 3.1) and the stochastic approach (Section 3.2). We present numerical results in Section 4 and conclusions and future research directions in Section 5.

2. Problem description

We consider the system constituted by two cylinders in tandem exposed to a uniform flow, as depicted in Figure 1. The two-dimensional incompressible flow of a viscous Newtonian fluid is considered; two identical rigid cylinders are mounted elastically in the domain such that they are free to vibrate perpendicularly to the flow direction (1 DoF). The flow is governed by the Navier-Stokes equations

$$\begin{aligned} \boldsymbol{\nabla}\cdot\boldsymbol{u} &= 0 \\ \frac{\partial \boldsymbol{u}}{\partial t} + (\boldsymbol{u}\cdot\boldsymbol{\nabla})\,\boldsymbol{u} &= -\frac{1}{\rho}\boldsymbol{\nabla} p + \frac{1}{Re}\boldsymbol{\nabla^2 u}, \end{aligned} \tag{2.1}$$

where $\boldsymbol{u} = (u, v)^{\mathrm{T}}$ is the velocity field, p is the pressure, ρ is the fluid density, and t is the time coordinate. The Reynolds number, Re, is defined as

$$Re = \frac{\rho U D}{\mu}, \tag{2.2}$$

where D is the cylinder diameter, U is the undisturbed upstream velocity, and μ is the dynamic viscosity of the fluid. The no-slip condition is imposed on the cylinders' surfaces Γ_i as

$$\boldsymbol{u}(\boldsymbol{x}, t) = \frac{\mathrm{d}\boldsymbol{X}_i^{cg}}{\mathrm{d}t}, \quad \text{for} \quad \boldsymbol{x} \in \Gamma_i(t), \tag{2.3}$$

where $\boldsymbol{x} = (x, y)^{\mathrm{T}}$ denotes the spatial coordinate, and $\boldsymbol{X}_i^{cg}$ is the location of the center of gravity of the ith cylinder.

The motion of the generic ith cylinder is described by Newton's second law

$$m\frac{\mathrm{d}^2\boldsymbol{X}_i^{cg}}{\mathrm{d}t^2} + k(\boldsymbol{X}_i^{cg} - \boldsymbol{X}_i^0) = \boldsymbol{F}_i(t), \tag{2.4}$$

where m is the mass, which is equal for both cylinders, $\boldsymbol{X}_i^0$ is the spring neutral position, k is the spring stiffness (identical for the two cylinders), and $\boldsymbol{F}_i$ is the force exerted by the fluid. This contribution comes from the integration of the viscous and pressure distributions over Γ_i, as a function of time. A more realistic model should also include the structural damping, but because we are interested in the most critical condition, i.e., the one that exhibits the most intense vibrations, neglecting the damping is considered to be a reasonable idealization. By introducing the natural frequency f as

$$f = \frac{1}{2\pi}\sqrt{\frac{k}{m}}, \tag{2.5}$$

we are able to define a critical parameter, namely the reduced velocity

$$U_{red} = \frac{U}{fD}. \tag{2.6}$$

The goal of the present study is to analyze the response of the system for a set of reduced velocities ranging from 4 to 8 (this range is the same as the one used in Borazjani & Sotiropoulos 2009). For the entire envelope of reduced velocities, we are interested in quantifying the effect of a non-exact knowledge of the relative locations of the two neutral positions. More precisely, we consider as a nominal condition the one studied in Borazjani & Sotiropoulos (2009), in which the horizontal distance L_x between the centers of the cylinder is $L_x/D = 1.5$, and we model it as a uniformly distributed random variable. We use a variation of $\pm 4\%$ around the nominal value, which leads to $L_x/D \sim \mathcal{U}(1.44, 1.56)$. The vertical distance between the two resting cylinders' centers is also modeled as a uniform random variable, and it is set to $L_y/D \sim \mathcal{U}(-0.05053, +0.05053)$.

3. Numerical setting

The overall numerical procedure is constituted by a set of deterministic computational fluid dynamics (CFD) instances followed by an Uncertainty Quantification (UQ) step which, by making use of those simulations, enables us to study the variability of the system over the stochastic space.

3.1. *Deterministic CFD simulations*

The governing equations are discretized in space using second-order-accurate central differences on a Cartesian staggered grid. The time discretization uses an explicit Adams–Bashforth scheme for the non-linear terms and an implicit Crank–Nicolson scheme for the viscous ones,

$$\frac{\hat{\boldsymbol{u}} - \boldsymbol{u}^n}{\Delta t} = -\alpha\boldsymbol{\nabla}p^n + \gamma\, H^n + \rho\, H^{n-1} + \frac{\alpha}{2\,Re}\,\nabla^2\left(\hat{\boldsymbol{u}} + \boldsymbol{u}^n\right), \tag{3.1}$$

where $\boldsymbol{u}^n$ denotes the velocity at the old time n; $\hat{\boldsymbol{u}}$ is the intermediate solution; Δt is the time step; H contains the non-linear terms; and α, γ, and ρ are the constants of the Adams–Bashforth/Crank–Nicolson scheme (Verzicco & Orlandi 1996). The resulting system is solved using a fractional-step method to obtain the intermediate non-solenoidal velocity field $\hat{\boldsymbol{u}}$. To get a divergence-free velocity field, a scalar quantity φ is introduced

such that

$$\boldsymbol{u}^{n+1} = \hat{\boldsymbol{u}} - \alpha\,\Delta t\,\boldsymbol{\nabla}\varphi. \tag{3.2}$$

By applying the discrete divergence operator to the equation above, an elliptic equation for φ is obtained and the large-banded matrix, associated with the elliptic equation, is reduced to a penta-diagonal matrix using trigonometric expansions (FFTs) in the spanwise direction. The resulting Helmholtz equations are inverted using the FISHPACK package (Swartzrauber 1974). Finally, the pressure field is computed as

$$p^{n+1} = p^n + \varphi - \frac{\alpha\,\Delta t}{2\,Re}\,\nabla^2\varphi. \tag{3.3}$$

To account for the presence of the moving bodies inside the domain, a direct forcing Immersed Boundary (IB) technique (Mittal & Iaccarino 2005) is employed, based on a versatile Moving Least Squares (MLS) reconstruction (Vanella & Balaras 2009). On the basis of the alternative direct-forcing scheme suggested by Uhlmann (2005), the forcing is computed on the Lagrangian markers laying on the immersed surface, so as to satisfy the boundary condition, and then transferred to the Eulerian grid points. The MLS approximation is the key ingredient for building a transfer function between the Eulerian and Lagrangian grids that can also provide a smooth solution in the presence of arbitrarily moving/deforming bodies. The procedure consists of the following steps:

(*a*) Compute the intermediate velocity $\hat{\boldsymbol{u}}$ from Eq. (3.1) in all the ne Eulerian grid points surrounding a Lagrangian point in its support domain. Here, the support domain is centered on the Lagrangian point and extends over $\pm 1.6\Delta x_i$, where Δx_i is the local grid size in the ith direction. In this way, 9 points are considered in two dimensions.

(*b*) Compute the velocity at all the Lagrangian grid points corresponding to the non-solenoidal velocity field according to

$$\hat{\boldsymbol{U}}(\boldsymbol{x}) = \sum_{k=1}^{ne} \psi_k^l(\boldsymbol{x})\,\hat{\boldsymbol{u}}_k, \tag{3.4}$$

where ψ is the transfer operator containing the shape functions and obtained by means of a MLS approximation.

(*c*) Calculate the volume force $\boldsymbol{F}$ at all Lagrangian grid points, in order to get the desired velocity $\boldsymbol{U}_b$ at the boundary as

$$\boldsymbol{F} = \frac{\boldsymbol{U}_b - \hat{\boldsymbol{U}}}{\Delta t}. \tag{3.5}$$

(*d*) Transfer $\boldsymbol{F}$ to the k Eulerian grid points associated with each Lagrangian grid point, using the same shape functions used in the interpolation procedure, properly scaled by a factor c_l, which is determined by imposing that the total force acting on the fluid is not changed by the transfer

$$\boldsymbol{f}^k = \sum_{l=1}^{nl} c_l\,\psi_k^l \boldsymbol{F}_l; \tag{3.6}$$

nl indicates the number of Lagrangian points associated with the Eulerian point k. One can also verify that the above scheme guarantees the equivalence of total torque between the Eulerian and Lagrangian computational grids (Vanella & Balaras 2009).

(*e*) Correct the intermediate velocity by means of the forcing, so as to satisfy the boundary conditions at the immersed body

$$\boldsymbol{u}^* = \hat{\boldsymbol{u}} + \Delta t\, \boldsymbol{f}; \tag{3.7}$$

this velocity field is not divergence-free and is projected into a divergence-free space by applying the pressure correction that satisfies the Poisson equation.

The forces and moments acting on the immersed body are calculated in time by integrating the pressure and viscous stresses over the immersed body surface. Given the surface discretization by nl triangular elements, one has

$$\boldsymbol{F}(t) = \sum_{l=1}^{nl} (\boldsymbol{\tau}_l \cdot \boldsymbol{n}_l - p_l \boldsymbol{n}_l)\, S_l \quad \text{and} \quad \boldsymbol{M}(t) = \sum_{l=1}^{nl} [\boldsymbol{r}_l \times (\boldsymbol{\tau}_l \cdot \boldsymbol{n}_l - p_l \boldsymbol{n}_l)]\, S_l, \tag{3.8}$$

where nl is the number of Lagrangian points; $\boldsymbol{\tau}_l$ and p_l are the viscous stress tensor and pressure, evaluated at the centroid of each triangle (location of the Lagrangian marker, l); $\boldsymbol{r}_l$ is the distance of the Lagrangian point from the centroid of the body; $\boldsymbol{n}_l$ and S_l are the normal unit vector and area of each triangle. To evaluate the pressure p_l and the velocity derivatives needed for the viscous stress tensor, for each Lagrangian marker a probe is created along its normal direction, at a distance h_l, equal to the averaged local grid size. Using the same MLS formulation described above, the pressure and velocity are evaluated on the probe location. The evaluation of the flow and particle motion at each time step is carried out by a strongly coupled fluid-structure interaction (FSI) scheme, because the prediction of the flow field and of the hydrodynamic loads requires the knowledge of the motion of the bodies and vice versa. An iterative implicit approach is considered, as reported in deTullio *et al.* (2009): for each time step, the convergence of the iterative procedure is verified by the condition $\mid \boldsymbol{V}_p^j - \boldsymbol{V}_p^{j-1} \mid < \epsilon$, where $\boldsymbol{V}_p^j$ indicates the body velocity at iteration j. In all our computations, a tolerance of $\epsilon = 10^{-6}$ was used, and the number of iterations required for convergence at each time step varied from 1 to 6, depending on the flow configuration. To avoid numerical instabilities in the FSI algorithm induced by the added mass effect, an under–relaxation of the forces (and moments) is employed, according to $\boldsymbol{F} = \gamma \boldsymbol{F}^j + (1-\gamma)\boldsymbol{F}^{j-1}$ with $\gamma = 0.9$. The computational domain considered is $[-8D, 24D] \times [-8D, 8D]$, and the flow comes in the horizontal direction from left to right. The tandem arrangement considered has $L_x/D = 1.5$, so that the front cylinder's center is placed in $(0, 0)$ and the rear one in $(1.5, 0)$. A non-uniform grid of 379×454 nodes is used, with a uniform grid spacing of $0.02D$ in the vicinity of the cylinder. The Lagrangian markers are distributed uniformly on the surface of the cylinder, with a spacing of $0.014D$, that is equal to 0.7 for the local Eulerian grid size in that area. The constant time step used is $\Delta t = 0.002\, D/U$, with $CFL = 0.4$. Inlet and outlet boundary conditions are imposed on the vertical boundaries, whereas free-shear wall conditions are imposed for the horizontal boundaries.

3.2. *Stochastic setting*

The UQ step is preformed using a non-intrusive Polynomial Chaos (PC) propagation. A set of sample points $\boldsymbol{\xi}^{(i)} \in \Xi \subset \mathbb{R}^2$, for $i = 1, \ldots, N$, is generated by means of a full tensorization of one-dimensional Clenshaw-Curtis (CC) points. In the following, we consider the random vector $\mathbb{R}^2 \ni \boldsymbol{\xi} = (\xi_1 = L_x/D, \xi_2 = L_y/D)^T$. The CC rule is nested, i.e., it is possible to refine the sample set re-using the previous points. Therefore, we performed a convergence study, although not reported here for brevity. After the convergence study, we found that 9 CC points ($N = 81$) for stochastic direction were enough to guarantee a satisfactory accuracy, as shown in the next section. Because the

problem is symmetric with respect to the neutral transversal distance L_y between the two cylinders, we performed only $N_{sim} = \frac{1}{2}(n_{1D}+1) \times n_{1D}$ numerical simulations, where n_{1D} is the number of 1D CC points. We consider in this study three distinct quantities of interest (QoI), namely the maximum displacement of the front $(y^{Fr}/D)_{max}$ and rear $(y^{Rear}/D)_{max}$ cylinder and the maximum vertical separation $(\Delta/D)_{max}$ that occurs during the entire time history. For a generic QoI $L^2(\Xi) \ni f : \Xi \to \mathbb{R}$, we can write

$$f(\boldsymbol{\xi}) = \sum_{k=0}^{P} \beta_k \Psi_k(\boldsymbol{\xi}), \tag{3.9}$$

where β_k and $\Psi_k(\boldsymbol{\xi})$ indicate the kth coefficient and the polynomial obtained by tensorization of 1D Legendre polynomials. The number of terms P in the expansion is related to the total polynomial order n chosen for the representation of f according to $P+1 = (n+2)!/(2\,n!)$. The orthogonality of the polynomial base is exploited to compute each coefficient as

$$\beta_k = \frac{\int_\Xi f(\boldsymbol{\xi})\Psi_k(\boldsymbol{\xi})p(\boldsymbol{\xi})\mathrm{d}\boldsymbol{\xi}}{\int_\Xi \Psi_k^2 \mathrm{d}\boldsymbol{\xi}} = \frac{\langle f(\boldsymbol{\xi}), \Psi_k(\boldsymbol{\xi})\rangle}{\langle \Psi_k(\boldsymbol{\xi}), \Psi_k(\boldsymbol{\xi})\rangle}, \tag{3.10}$$

where the operator $\langle\cdot\rangle$ denotes the L^2 inner product according to the joint probability density $p(\boldsymbol{\xi})$. All the integrals are evaluated using the same CC rule, such that

$$\langle f(\boldsymbol{\xi}), \Psi_k(\boldsymbol{\xi})\rangle = \sum_{i=1}^{N} f(\boldsymbol{\xi}^{(i)})\Psi_k(\boldsymbol{\xi}^{(i)})p(\boldsymbol{\xi}^{(i)})w_i, \tag{3.11}$$

where w_i is the quadrature weights obtained by tensorization of the one-dimensional CC quadrature weights.

4. Numerical results

The main goal of the present analysis is to quantify the probability of the occurrence of events related to the QoI defined above. This task involves the evaluation of probability density functions (PDFs), which in turn requires an assessment of the PC expansion accuracy. Specifically, the response surface, for each QoI, is obtained by Eq. (3.9), and this PC expansion can be sampled with a larger number of realizations to obtain a continuous representation (for the QoI) over the entire stochastic space Ξ. In this work we used a lattice of 1500 uniformly distributed points per direction. Hereafter, we refer to this continuous approximation as a metamodel of the QoI. For each QoI, the optimal polynomial order is identified by means of a convergence study. We considered total polynomial orders n ranging from 4 to 8, and we evaluated the L^1, L^2 and L^∞ norms according to

$$\begin{aligned}
err_{L^1} &= \frac{\sum_{i=1}^{N} \left| f(\boldsymbol{\xi}^{(i)}) - f_{\mathrm{true}}(\boldsymbol{\xi}^{(i)}) \right| p(\boldsymbol{\xi}^{(i)}) w_i}{\sum_{i=1}^{N} \left| f_{\mathrm{true}}(\boldsymbol{\xi}^{(i)}) \right| p(\boldsymbol{\xi}^{(i)}) w_i} \\
err_{L^2} &= \left(\frac{\sum_{i=1}^{N} f(\boldsymbol{\xi}^{(i)}) - f_{\mathrm{true}}(\boldsymbol{\xi}^{(i)}))^2 p(\boldsymbol{\xi}^{(i)}) w_i}{\sum_{i=1}^{N} f_{\mathrm{true}}^2(\boldsymbol{\xi}^{(i)}) p(\boldsymbol{\xi}^{(i)}) w_i} \right)^{1/2} \\
err_{L^\infty} &= \max \left| \frac{(f(\boldsymbol{\xi}^{(i)}) - f_{\mathrm{true}}(\boldsymbol{\xi}^{(i)}))}{f_{\mathrm{true}}(\boldsymbol{\xi}^{(i)})} \right|_i,
\end{aligned} \tag{4.1}$$

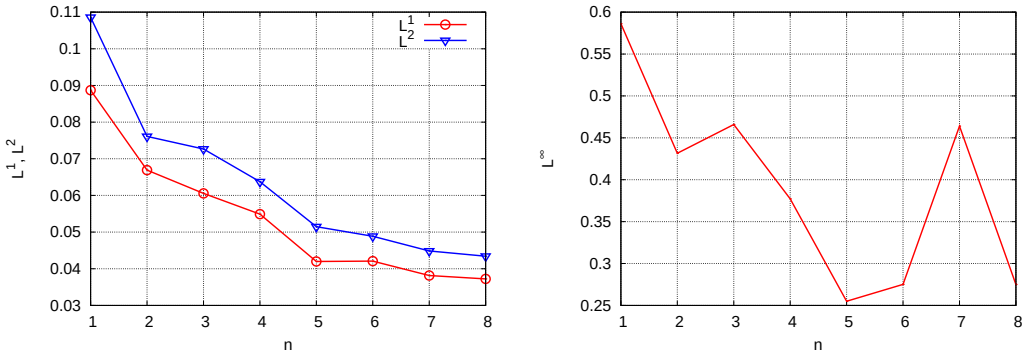

(a) (b)

FIGURE 2. Maximum displacement for the front cylinder at $U_{red} = 4$. The L^1 and L^2 norms are reported in (a) and the L^∞ norm is reported in (b) and they are computed according to Eq. (4.1).

where f_{true} denotes the value obtained from the numerical simulations, whereas f is obtained from Eq. (3.9). The results of this convergence study are not reported here for brevity, but we report in Figure 2 a representative situation of the convergence of the metamodel while total polynomial degree increases. In Figure 2 we can see how the L^1 and L^2 are monotonically decreasing with n, whereas the L^∞ has a less regular behavior. This feature is associated with the under- or over-shootings that may happen if the polynomial degree is too high, i.e., the model includes a spectral content that is too high with respect to the accuracy of the quadrature rule employed to compute each single coefficient. The convergence of the L^1 and L^2 norms is instead more regular because the metamodel continues to converge in a mean square sense even in the presence of local spurious oscillations. From a practical standpoint, in a situation like the one reported in Figure 2, the optimal total polynomial order is set to $n = 5$. This polynomial order corresponds to a minimum for the L^∞ norm, while the L^1 and L^2 norms are still diminishing.

4.1. *Front cylinder displacement* $(y^{Fr}/D)_{max}$

The metamodel corresponding to $n = 5$ for the maximum displacement of the front cylinder $(y^{Fr}/D)_{max}$ is reported in Figure 3 for the reduced velocities $U_{red} = 4, 5, 6$, and 8. The true values of the simulations are also reported to show the agreement between the true samples and the metamodels. Because the stochastic space represents the neutral position of the rear cylinder, if we consider the horizontal separation between the cylinders, it is possible to note that for $U_{red} \leq 6$ the smallest displacements are obtained when the rear cylinder is placed very close to the front one. The opposite behavior is obtained for $U_{red} = 8$, i.e., in this case the smallest amplitude is obtained for the rear cylinder placed at $L_x/D = 1.56$. This behavior suggests that the wake structure of the front cylinder plays a major role in enhancing the vertical vibrations of the cylinder. Therefore, when the rear cylinder is placed more closely to the front one, it is reasonable to suppose that its interactions with the wake are damping this enhancing effect. Figure 3 also reveals that the influence of the vertical separation between the two neutral positions increases with U_{red}. For U_{red} equal to 4 and 5, $(y^{Fr}/D)_{max}$ is mainly governed by changes in the initial horizontal separation, whereas at U_{red} equal to 6 and 8, local features related to the initial vertical separation appear. For instance, in Figure 3(d) the local maxima of the function $(y^{Fr}/D)_{max}$ occur for $L_x/D \approx 1.47$ and $L_y/D \approx \pm 0.03$ or the local minima are

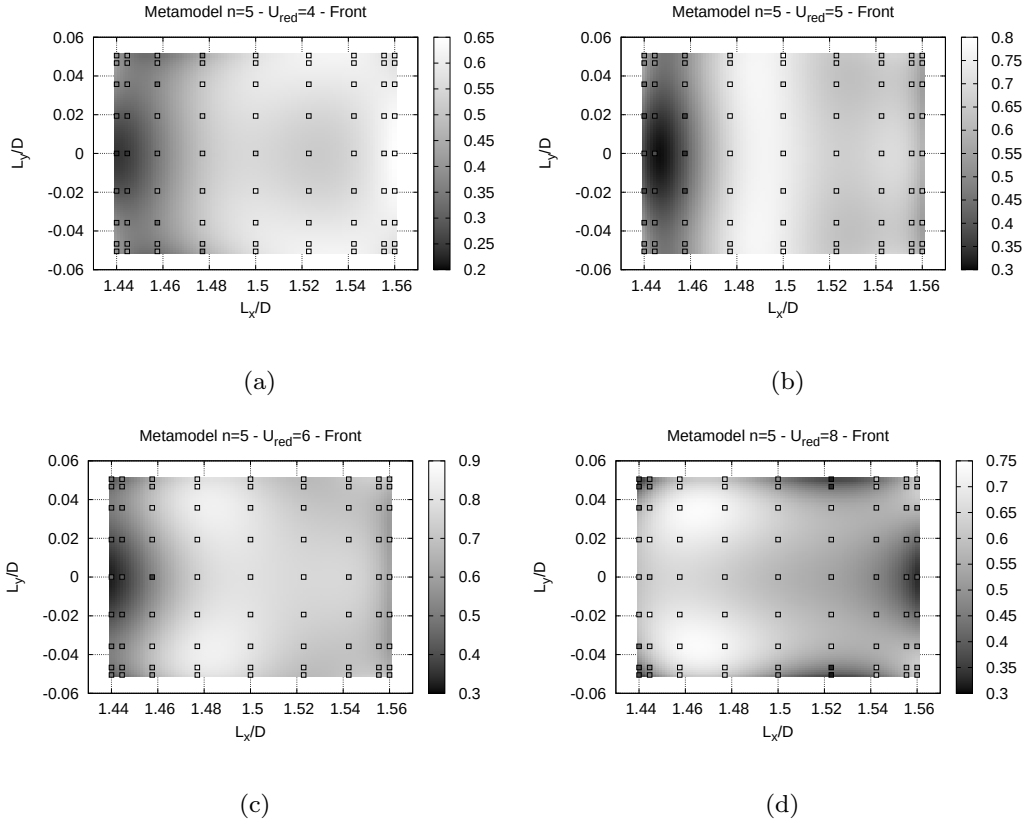

FIGURE 3. Front cylinder maximum displacement $(y^{Fr}/D)_{max}$. Four reduced velocities are reported, namely $U_{red} = 4$ (a), $U_{red} = 5$ (b), $U_{red} = 6$ (c), and $U_{red} = 8$ (d). The realizations obtained from the numerical simulations are also reported for comparison. All the metamodels are obtained by using a total polynomial order $n = 5$.

obtained for $L_x/D \approx 1.52$ and $L_y/D \approx \pm 0.05$. This analysis is confirmed by an ANalysis Of VAriance (ANOVA) reported in Figure 4(a). More precisely, hereafter we report the so called Sobol indices which are defined, for each term, as its conditional variance and the variance itself. We refer the reader to Sobol (2001) and Creastaux *et al.* (2009) for further details on the ANOVA decomposition and its evaluation using a PC approach. All the contributions remain constant for $U_{red} = 4$ and 5; however, a further increase in the reduced velocity results in a doubling of the mixed contribution value, which reaches approximately 0.10, whereas the contribution related to the horizontal separation decreases to a value of 0.7 and the vertical separation contribution increases up to approximately 0.15. These results can be further explained if we consider the discussions reported in Borazjani & Sotiropoulos (2009). The authors, for the reduced velocity $U_{red} = 8$, identify in the gap flow (i.e., a flow with velocities as high as the freestream velocity U) the main phenomenon driving the entire flow dynamics. It is reasonable to suppose that placing the rear cylinder in a position with $L_y/D \neq 0$ would affect the gap flow having strong consequences on the entire dynamics of the system; hence, there is a larger sensitivity of the system to L_y/D for $U_{red} = 8$.

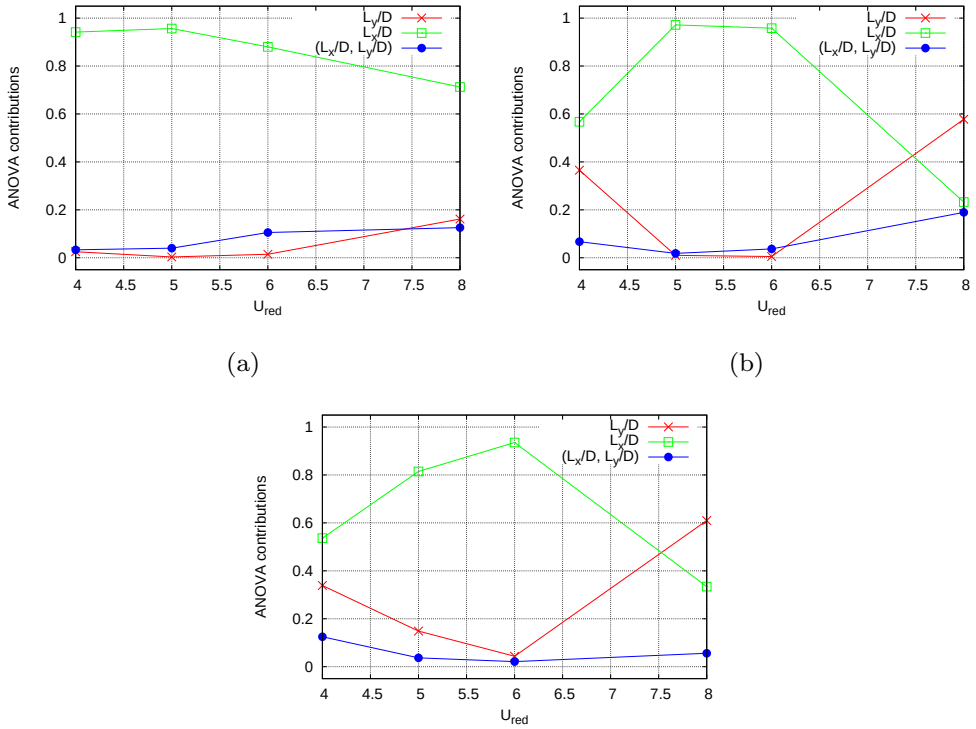

FIGURE 4. ANOVA decomposition for the maximum displacement of the front $(y^{Fr}/D)_{max}$ (a), rear cylinder $(y^{Fr}/D)_{max}$ (b), and maximum vertical separation $(\Delta/D)_{max}$ (c) as a function of the reduced velocity U_{red}.

4.2. *Rear cylinder displacement* $(y^{Rear}/D)_{max}$

The metamodel for the maximum displacement of the rear cylinder $(y^{Rear}/D)_{max}$ is reported in Figure 5 for all the reduced velocities. Figure 5 reveals a much more complex behavior with respect to its counterpart relative to the front cylinder. The greater complexity of this QoI with respect to $(y^{Fr}/D)_{max}$ is also evident from Figure 4(b) where the ANOVA decomposition is reported. For the intermediate reduced velocities $U_{red} = 5$ and 6, the response is dominated by the horizontal separation L_x/D, whereas for the two extreme reduced velocities the values of the vertical separation's contributions reach approximately 0.4 and 0.6 for $U_{red} = 4$ and 8, respectively. The ANOVA analysis legitimizes our hypothesis of the existence of a very peculiar flow regime for reduced velocities around 5.5; moving away from this condition, the flow regime abruptly changes. Another indication of the existence of such a flow regime is the transition between reduced velocities for which the minimum amplitude $(y^{Rear}/D)_{max}$ occurs for high L_x/D, Figures 5(a,b), and the ones for which the minimum amplitudes occur for low values of L_x/D, Figures 5(c,d). In addition, the two extreme reduced velocities considered in this work reveal substantially different features. For the low velocity $U_{red} = 4$, the effect of the horizontal separation L_x/D is still predominant, attaining a value of 0.6, compared with 0.4 reached by the contribution of L_y/D; at $U_{red} = 8$, the predominant contribution is the one related to L_y/D, which reaches 0.6. In this latter case, the contribution related

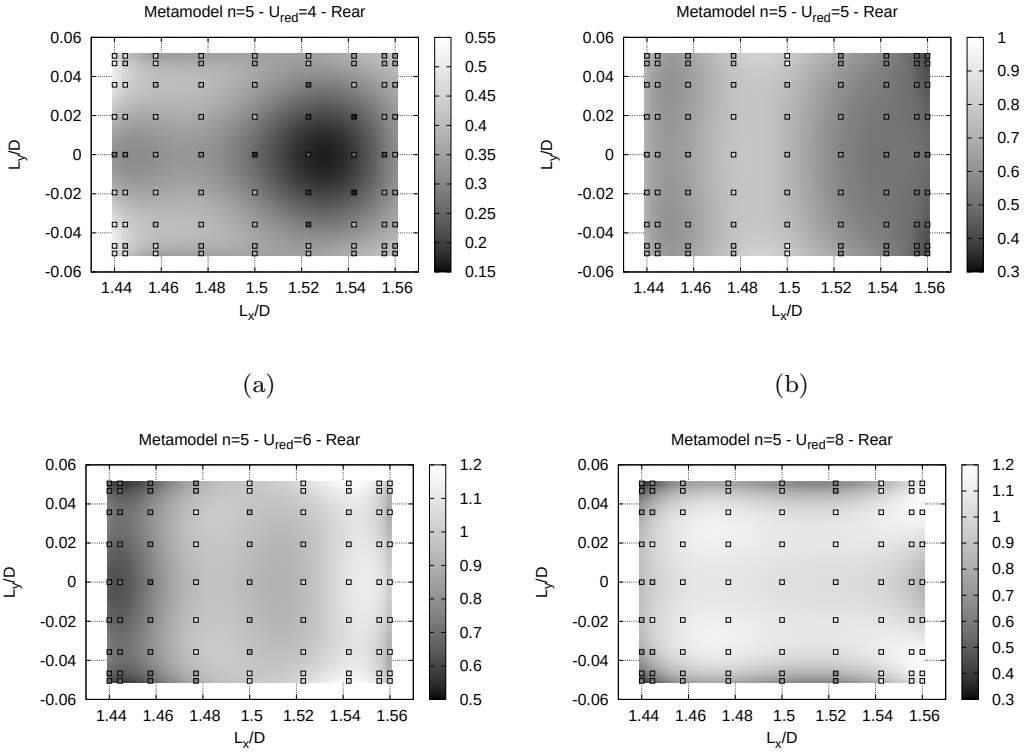

FIGURE 5. Rear cylinder maximum displacement $(y^{Rear}/D)_{max}$. Four reduced velocities are reported, namely $U_{red} = 4$ (a), $U_{red} = 5$ (b), $U_{red} = 6$ (c), and $U_{red} = 8$ (d). The realizations obtained from the numerical simulations are also reported for comparison. All the metamodels are obtained by using a total polynomial order $n = 5$.

to L_x/D is only 0.2. Moreover, whereas for $U_{red} = 4$ the minimum of $(y^{Rear}/D)_{max}$ is reached along the line $L_y/D = 0$, for $U_{red} = 8$ it is necessary to move the rear cylinder away from the front cylinder's wake to obtain the minimum response. A preliminary possible interpretation for this behavior is that for low reduced velocities the front cylinder wake effect is to damp the rear cylinder vibrations. On the other hand, when the reduced velocity is higher, then the front wake can excite the rear cylinder's vibrations. Moving the rear cylinder away from the front wake removes this enhancing effect, which in turn results in small amplitudes. Although, the analysis of these complex mechanisms is far beyond the scope of the present investigation, however, and needs to be supported by using more detailed analysis of the instantaneous vorticity fields obtained during the motion for the different reduced velocities.

4.3. *Maximum vertical separation* Δ/D

The polynomial metamodel for $(\Delta/D)_{max}$ is reported in Figure 6. For this QoI, the minimum values are located near the corners for $U_{red} = 4$ and 5, whereas at $U_{red} = 6$ they are obtained for low values of the horizontal separation L_x/D almost independently of the vertical separation L_y/D. On the contrary, for $U_{red} = 8$, the minimum values of the response occur for low values of the horizontal separation L_x/D and high (absolute) values

of the vertical separation L_y/D. For all the reduced velocities, a local maximum corresponds, approximately, to the reference condition; this behavior confirms that placing the rear cylinder with a horizontal separation around $L_x/D = 1.5$ causes strong interactions between the cylinders. The ANOVA analysis, reported in Figure 4(c), reveals that for the reduced velocity $U_{red} = 6$, the dynamics of the system is dominated by the horizontal separation, whereas moving away from this condition increases the relevance of the vertical separation L_y/D. In particular, as already seen for $(y^{Rear}/D)_{max}$, for a reduced velocity $U_{red} = 8$, the contribution associated with the vertical separation becomes more relevant. This feature allowed us to conjecture that a link exists between the vertical separation and the gap flow that occurs and that dominates the dynamics of the system for $U_{red} = 8$. On the contrary, for the lowest reduced velocity, $U_{red} = 4$, according to Borazjani & Sotiropoulos (2009) the flow never impinges the rear cylinder, but rather passes around it. However, when the neutral position of the rear cylinder corresponds to a large (absolute) value for L_y/D, it is possible to suppose that this cylinder becomes exposed to the flow during the oscillation cycles and also that a gap flow may be established by obtaining a mechanism closer to the one corresponding to $U_{red} = 8$. At this point, we cannot further support these preliminary interpretations without further analyses of the instantaneous pressure and velocity fields of the flow. However, such analyses are beyond the scope of the present contribution.

4.4. *Front cylinder and real cylinder envelope*

The realizations (1500^2) used for obtaining the behavior of the different QoIs presented in the previous sections can also be used to compute PDFs. One of the main findings in Borazjani & Sotiropoulos (2009) is that for low reduced velocities the amplitudes of vibration of the rear cylinder are larger than the ones of the front cylinder. Figure 7(a) illustrates the box plots corresponding to 25%, 50%, and 75% within the whiskers bars denoting the values of 5% and 95% as a function of the reduced velocity. For the lowest reduced velocity, the probability is higher of having larger oscillations for the front cylinder with respect to those of the rear cylinder, but with a probability higher than 50% the maximum oscillations of the rear cylinder are falling in the interval 5-25% of probability for $(y^{Fr}/D)_{max}$. For the reduced velocity $U_{red} = 5$, the confidence intervals are superimposed. In particular the tighter one, which corresponds to the oscillations of the rear cylinder, is almost entirely contained in the one corresponding to the front cylinder. The situation changes for the large reduced velocities, $U_{red} = 6$ and 8. In particular for $U_{red} = 6$, the interval 25-95% of the front cylinder's response is almost entirely contained in the interval 5-20% of the rear cylinder. Finally, the two confidence intervals become completely disjointed for the largest reduced velocity, $U_{red} = 8$. This analysis suggests that the conclusion reported in Borazjani & Sotiropoulos (2009) correspond to the nominal condition, but whenever the rear cylinder can be placed into the domain with an uncertain position, a low probability of occurrence of having larger oscillations for the front cylinder than for the rear one can only be claimed for the highest reduced velocity, $U_{red} = 8$. In all the other cases, a non-negligible probability exists of having larger amplitudes of vibrations for the front cylinder with respect to those of the rear cylinder.

4.5. *Front cylinder: comparison with isolated cylinder*

The work in Borazjani & Sotiropoulos (2009) also focuses on the difference between the response of the front cylinder and that of an isolated cylinder exposed to the same flow. In particular, it is claimed that larger amplitudes occur for the tandem arrangement

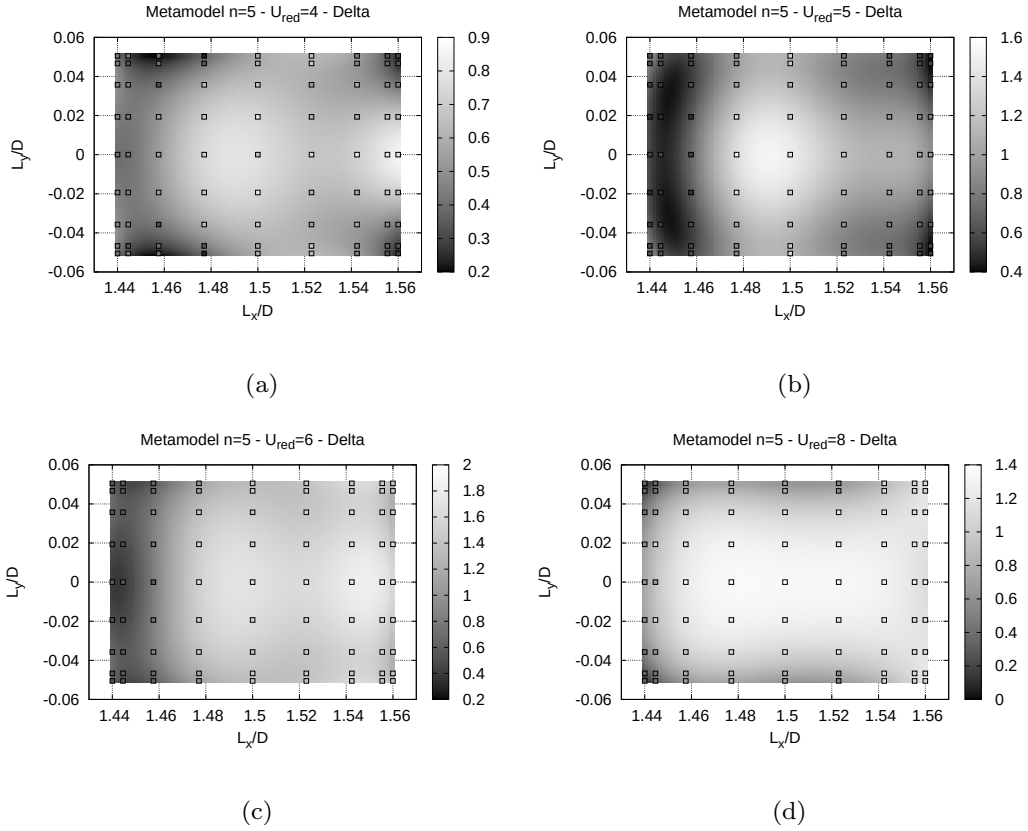

FIGURE 6. Maximum separation $(\Delta/D)_{max}$ between the two cylinders. Four reduced velocities are reported, namely $U_{red} = 4$ (a), $U_{red} = 5$ (b), $U_{red} = 6$ (c), and $U_{red} = 8$ (d). The realizations obtained from the numerical simulations are also reported for comparison. All the metamodels are obtained by using a total polynomial order $n = 5$.

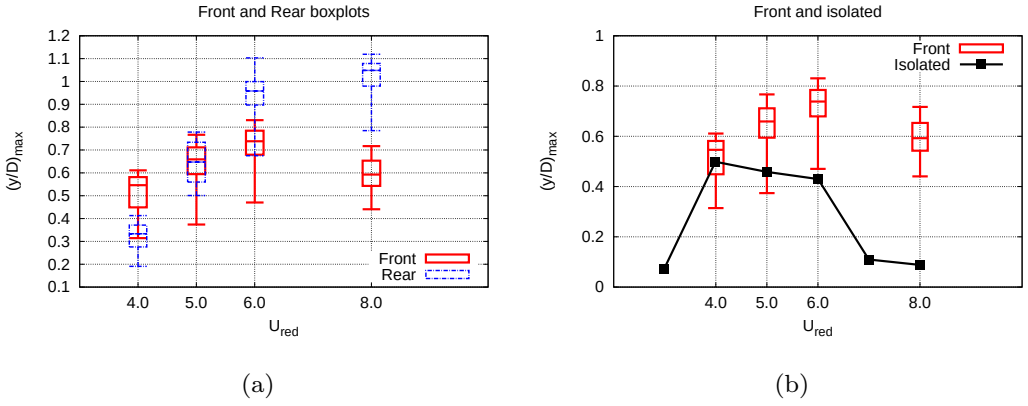

FIGURE 7. Box plots (and whiskers) for the response of front and rear cylinder (a) and the front cylinder maximum amplitude of oscillation $(y^{Fr}/D)_{max}$ compared to the maximum amplitude reached by an isolated cylinder (b). Both the curves are reported as a function of the reduced velocity.

U_{red}	$(y^{iso}/D)_{max}$	$P\left(\left(y^{Fr}/D\right)_{max} < \left(y^{iso}/D\right)_{max}\right)$	$P\left(\left(y^{Fr}/D\right)_{max} > \left(y^{iso}/D\right)_{max}\right)$
4	0.499	0.321	0.678
5	0.458	0.136	0.863
6	0.430	0.031	0.969
8	0.088	0.000	1.000

TABLE 1. Probability, for the front cylinder, of exceeding the maximum displacement of the isolated cylinder exposed to the same flow as a function of the reduced velocity U_{red}.

compared to the isolated cylinder and also that a wider lock-in region is present for the tandem arrangement. In this work, for all the reduced velocities considered in this study, we compared the confidence interval for the oscillations of the front cylinder with the amplitude of oscillation of an isolated cylinder. These results are reported in Figure 7(b). In addition, we quantified the probability of having larger oscillations for the front cylinder versus an isolated cylinder. These probabilities are reported in Table 1. From Table 1, we can identify the reduced velocity $U_{red} = 6$ as the one for which the probability of having larger oscillations for the front cylinder decreases to a value lower than a threshold value, set as 5%. For all the other velocities, $U_{red} < 6$, a non-negligible probability of occurrence of larger oscillations for the isolated cylinder compared to the front cylinder exists. This kind of result can be of practical importance when designing a structure considering each structural element as isolated, and it is necessary to identify margins of safety with respect to the random relative positions between elements. These results also suggest that large reduced velocities are needed for guaranteeing that the front cylinder is always subject to oscillations that are larger than the corresponding ones of an isolated element.

5. Summary and perspectives

A preliminary stochastic analysis of the VIV of two oscillating cylinders in the proximity-wake interference region is presented. A numerical analysis is performed on a configuration consisting of two identical rigid cylinders placed in tandem. The cylinders are elastically mounted and, therefore, are free to vibrate, transversally to the flow, in response to flow-induced forces. An imperfect knowledge of the relative resting distance between the cylinders is considered a source of uncertainty in the system. The vibration of this arrangement is studied for flows corresponding to reduced velocities ranging from 4 to 8. Two uniform random variables are used to prescribe the uncertain resting relative position of the two cylinders. Different quantities of interest, namely the maximum amplitude of oscillation of the front and rear cylinders and their maximum (vertical) separation are considered. The statistics obtained for the QoI enable us to provide a quantification of the probability of occurrence for the main findings reported in Borazjani & Sotiropoulos (2009): (i) larger amplitude of motion for the tandem arrangement compared to an isolated cylinder, (ii) larger oscillation for the front cylinder compared to the rear one for low reduced velocities, and (iii) significantly larger vibrations for the rear cylinder compared to the front one when the reduced velocity is above a certain threshold. The PC expansion is also adopted to evaluate the sensitivity of the system to the contributions of the horizontal and vertical separations between the neutral positions of the cylinders by means of an ANOVA decomposition. The ANOVA analysis

reveals that the role played by the horizontal and vertical separation between the two cylinders is a function of the reduced velocity. Notably, the contribution of the horizontal separation is always the most important one for all the QoI and the reduced velocities considered in this study, with the exception of the maximum amplitude of oscillation of the rear cylinder and the maximum separation between the cylinders at the reduced velocity $U_{red} = 8$, for which the main contribution to the variance comes from the vertical separation L_y/D. Moreover, the ANOVA analysis shows a critical regime, around a reduced velocity of approximately 5.5, which is identified by the peak of the variance contribution associated with the horizontal separation between the cylinders. Moving away from this critical condition, the contribution of the vertical separation to the variance becomes, increasingly, more important. Current research directions are focused on the analysis of the evolution of the vorticity and pressure field to gain a deeper understanding of the physical mechanisms that are conjectured to be responsible for the transition between the different regimes revealed by the preliminary stochastic analysis reported in this brief.

REFERENCES

Borazjani, I. & Sotiropoulos, F. 2009 Vortex-induced vibrations of two cylinders in tandem arrangement in the proximity-wake interference region. *J. Fluid Mech.* **621**, 321–364.

Creastaux, T., Le Maître, O., Martinez, J.M. 2009 Polynomial chaos expansion for sensitivity analysis. *Reliab. Eng. Syst. Safe.* **94**(7), 1161–1172.

de Tullio, M.D., Cristallo, A., Balaras, E. & Verzicco, R. 2009 Direct numerical simulation of the pulsatile flow through an aortic bileaflet mechanical heart valve. *J. Fluid Mech.* **622**, 259-290.

Griffin, O.M. & Ramberg S.E. 1982 Some recent studies of vortex shedding with application to marine tubulars and risers. *J. Energy Resour. Technol.: Trans. ASME* **104**(1), 2–13.

Mittal, R. & Iaccarino, G. 2005 Immersed boundary methods. *Annu. Rev. Fluid Mech.* **37**, 239-261.

Sobol, I.M. 2001 Global sensitivity indices for nonlinear mathematical models and their Monte Carlo estimates. *Math. Comput. Simulat.* **55**, 271–280.

Swartzrauber, P.N. 1974 A direct method for the discrete solution of separable elliptic equations. *SIAM J. Numer. Anal.* **11**, 1136-1150.

Uhlmann, M. 2005 An immersed boundary method with direct forcing for the simulation of particulate flows. *J. Comp. Phys.* **209**, 448-476.

Vanella, M. & Balaras, E. 2009 A moving-least-squares reconstruction for embedded-boundary formulations. *J. Comp. Phys.* **228**, 6617-6628.

Verzicco, R. & Orlandi, P. 1996 A finite difference scheme for three-dimensional incompressible flows in cylindrical coordinates. *J. Comp. Phys.* **123**, 402–413.

Williamson, C.H.K. & Govarghan, R. 2004 Vortex-induced vibrations. *Annu. Rev. Fluid Mech.* **36**, 413–455.

Williamson, C.H. & Roshko, A. 1988 Vortex formation in the wake of an oscillating cylinder. *J. Fluid Struct.* **2**, 355–381.

Zdravkovich, M.M. & Pridden, D.L. Interference between two circular cylinders, series of unexpected discontinuities. *J. Ind. Aerodyn.* **2**, 255–270.